International Journal of Nanomedicine Dovepress

Open Access Full Text Article ORIGINAL RESEARCH

Combination of Losartan and Platinum Nanoparticles with Photothermal Therapy Induces Immunogenic Cell Death Effective Against Neuroblastoma

Xiaojun Zhang[1,*], Ying Zhao[2,*], Zhaogang Teng[3], Tangyao Sun[3], Jun Tao[3], Jiang Wu[4], Yu Wang[3], Fan Qiu[4], Feng Wang[4]

[1]Department of Radiology, Children's Hospital of Nanjing Medical University, Nanjing, 210018, People's Republic of China; [2]Department of Radiology, Nanjing First Hospital, Nanjing Medical University, Nanjing, 210006, People's Republic of China; [3]Key Laboratory for Organic Electronics & Information Displays and Jiangsu Key Laboratory for Biosensors, Institute of Advanced Materials, Jiangsu National Synergetic Innovation Centre for Advanced Materials, Nanjing University of Posts and Telecommunications, Nanjing, 210023, People's Republic of China; [4]Department of Nuclear Medicine, Nanjing First Hospital, Nanjing Medical University, Nanjing, 210008, People's Republic of China

*These authors contributed equally to this work

Correspondence: Fan Qiu; Feng Wang, Email qiufan0928@163.com; fengwangcn@hotmail.com

Introduction: Photothermal therapy (PTT) is a promising therapeutic procedure with minimal side effects, which can not only kill tumor directly but also cause immunogenic cell death (ICD). However, most solid tumors, including neuroblastoma, are abundant in fibroblasts, which limit the penetration and delivery of nanoparticles. Losartan is an antihypertensive drug approved by the FDA, and it has been proved to have the effect of breaking down excessive ECM network.

Methods: In this study, we investigated the application and potential mechanism of the combination of mesoporous platinum nanoparticles (MPNs) and losartan in the PTT of neuroblastoma by establishing neuroblastoma models in vitro and in vivo.

Results: Compared to the MPNs group without 808 nm laser irradiation, Neuro-2a cells pretreated with PTT and losartan showed lower survival rates, increased surface calreticulin, and higher release of HMGB1 and ATP. The group also exhibited the highest anti-tumor efficacy in vivo, with a tumor suppression ratio of approximately 80%. Meanwhile, we found that $CD3^+$ T cells, $CD4^+$ T cells and $CD8^+$ T cells from the peripheral blood of experimental group mice were significantly higher than control groups, and $CD8^+PD\text{-}1^+$ cells were significantly lower than those in MPNs + Los group and Los + laser group. And the expression of PD-1 and α-SMA in Neuro-2a tumors tissue was reduced. Furthermore, losartan could reduce damage of liver function caused by MPNs and laser treatment.

Conclusion: This study demonstrated that losartan-induced fibroblasts ablation increased the penetration of MPNs into tumors. Enhanced penetration allowed PTT to kill more tumor cells and synergistically activate immune cells, leading to ICD, indicating the great promise of the strategy for treating neuroblastoma in vivo.

Keywords: photothermal therapy, immunogenic cell death, neuroblastoma, losartan, extracellular matrix

Introduction

Neuroblastoma (NB) is the most common extracranial pediatric solid tumor, accounting for 15% of all pediatric cancer-related deaths.[1] NB is characterized by abundant tumor vasculature, rapid growth and early metastasis.[2,3] Most NB patients are at an advanced stage at the time of diagnosis.[4] Comprehensive treatments, including surgery, chemotherapy, radiotherapy, anti-GD2 therapy, and autologous stem cell transplantation, are commonly used in clinical settings. The unsatisfactory results of multiple existing treatments emphasize the need for additional therapeutic options.[5–8]

Received: 8 March 2024
Accepted: 30 September 2024
Published: 9 October 2024

Graphical Abstract

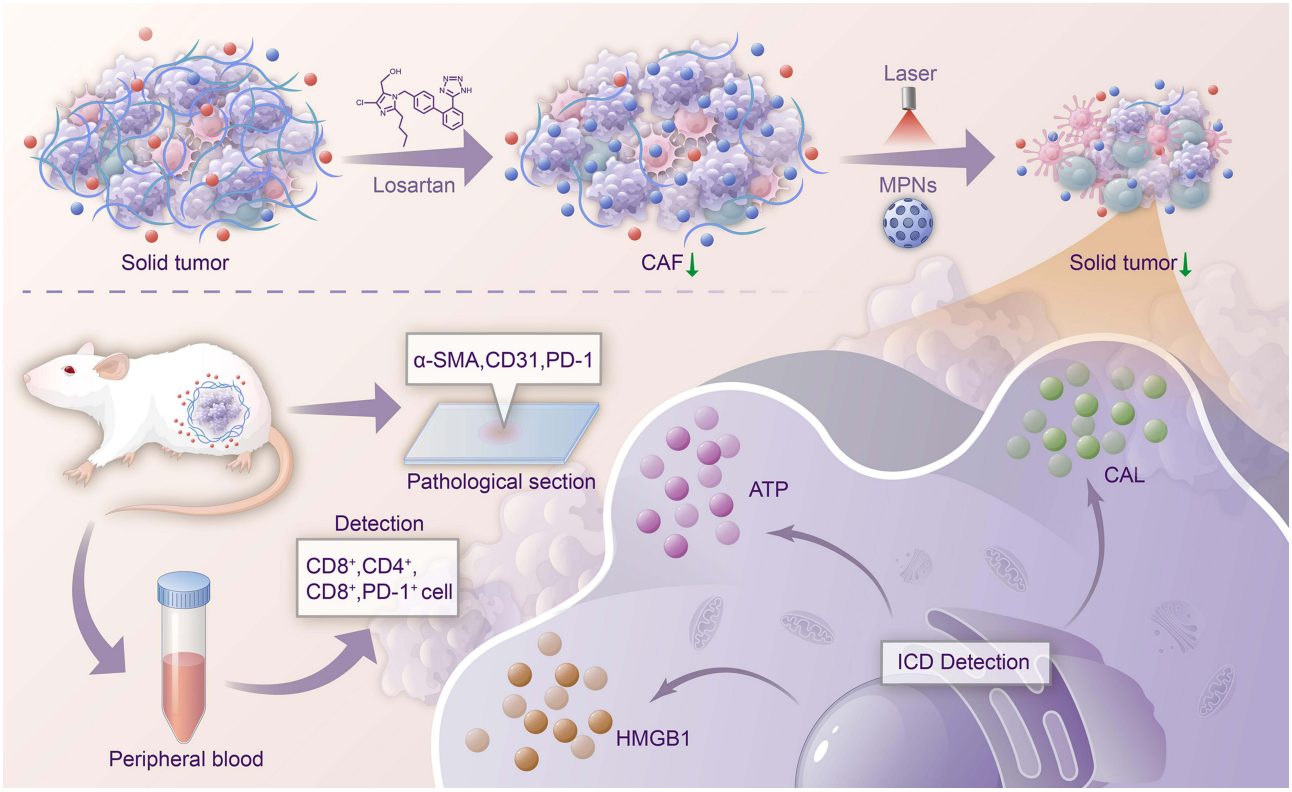

Photothermal therapy (PTT) is a promising therapeutic procedure with fewer side effects, shorter therapeutic schedules and higher efficacy compared to chemotherapy and radiotherapy.[9] PTT can not only eliminate tumor cells directly, but also release tumor antigens and endogenous adjuvants.[10] These endogenous adjuvants have the potential to increase tumor immunogenicity and thereby improve therapeutic responses, as it provides the potential for sustained therapeutic responses and immune memory to slow tumor recurrence and metastasis.[11,12] The immune system is easily bypassed by neuroblastoma,[13] and PPT is a good treatment for neuroblastoma due to its high selectivity, minimal invasiveness, and immunogenic effects. However, most solid tumors, including NB, are abundant in fibroblasts, which limit the penetration and delivery of nanoparticles.[14] The limited light penetration depth and insufficient distribution of photosensitizers in solid tumors lead to incomplete clearance of tumors by PPT.[15] Cancer-associated fibroblasts (CAFs) and CAFs-secreting extracellular matrix (ECM) are abundant in the tumor microenvironment (TME).[16] Collagen and hyaluronic acid make up most of the ECM in tumors.[17] The dense extracellular matrix decreases tumor perfusion, elevates interstitial fluid pressure (IFP), and is a barrier to drug transport.[18] Elevated IFP and hypoperfusion are hallmarks of the TME, and they pose major physiological barriers to the transport of drugs through the tumor vasculature, across the tumor blood vessel wall into the tumor interstitial space and through the interstitial space of the tumor.[19] Thus, reducing tumor fibroblasts and normalizing the TME can decrease fluid pressure and solid stress, enhancing drug delivery and PTT efficacy.

Common matrix metalloproteinase and bacterial collagenases reduce fibroblasts and matrix density but increase the risk of tumor progression and toxicity to normal tissues.[20] Losartan, an FDA-approved antihypertensive drug and angiotensin II type-1 receptor blocker (ARB), has a long history of safety. Losartan has been shown to have immunomodulatory and anti-fibrotic activity.[21] In vitro studies demonstrate that losartan and similar agents normalize tumor ECM and enhance tumor perfusion.[19] Chauhan et al reported that losartan improves anticancer drug and nanotherapeutic

distribution and efficacy.[22] A retrospective study showed that the angiotensin I-converting enzyme inhibitors (ACEIs)/ARBs in combination with gemcitabine may improve clinical outcomes in patients with advanced pancreatic cancer.[23] Another recent Phase 2 trial in pancreatic ductal adenocarcinoma showed encouraging results with neoadjuvant chemotherapy with losartan.[24]

Herein, we report the development of mesoporous platinum nanoparticles (MPNs) combined with losartan and the exploration of its use as an effective nanoplatform for targeted PTT of NB. MPNs were selected because of high stability and photothermal conversion efficacy (62.4%), excellent biocompatibility and surface chemistry.[25,26] MPNs has good biocompatibility, and there are even reports showing that it helps reduce the toxicity of chemotherapy drugs to normal tissues.[27] This study explores whether combining MPNs-based PTT with losartan enhances antitumor efficacy and investigates the underlying mechanisms. Our data indicate that combinational therapy with MPNs based PTT and losartan would enhance the anti-tumor effect of PTT through depletion of tumor fibroblasts and activating ICD. Losartan can modulate fibroblast and collagen to reduce tumor ECM, thereby enhancing the penetration of MPNs into tumors. This process results in robust PTT efficacy and activates $CD8^+$ T cell-mediated anti-tumor immunity. Furthermore, it has the potential to generate long-term anti-tumor immune memory and inhibit tumor recurrence and metastasis.

Materials and Methods

Pluronic F127 and L-ascorbic acid (L-AA, ≥99%) were obtained from Sigma-Aldrich (St. Louis, MO, USA). Chloroplatinic acid hexahydra ($H_2PtCl_6 \cdot 6H_2O$) and potassium bromide (KBr, ≥99.9%) were purchased from Sinopharm Chemical Reagent Co., Ltd. (Shanghai, China). CCK-8 kit and calcein AM/PI staining kit were purchased from Beyotime Biotech. Inc. (Shanghai, China). Anti-HMGB1 and anti-calreticulin were purchased from Abcam (Cambridge, UK). Alexa Fluor 488 anti-mouse CD4, PE/Cyanine7 anti-mouse CD45, PE anti-mouse CD3ε and APC/FireTM 750 anti-mouse CD8a were purchased from Biolegend Inc. (San Diego, CA). Anti-mouse PD-1 and anti-mouse α-SMA were purchased from Abcam (Cambridge, MA). Minimum essential medium (MEM) and fetal bovine serum (FBS) were purchased from Gibco (Life Technologies Corporation, Switzerland). Mouse high mobility group protein box-1 (HMGB-1) ELISA kit was purchased from Wuhan Huamei Biological Engineering Co., Ltd. (Wuhan, China). ATP content assay kit was purchased from Beijing Solarbio Science & Technology Co., Ltd. (Beijing, China).

Synthesis of Mesoporous Platinum Nanoparticles

First, 1.8 g of F127 and 4 g of KBr were completely dissolved in 60 mL of L-ascorbic acid (L-AA) water solution (0.1 M). Next, 1 mL of H_2PtCl_6 water solution (0.2 M) was added, and the solution was thoroughly mixed. The resulting solution was then placed in a water bath at 70 °C for 24 h. The obtained product was collected by centrifugation at 10000 rpm for 5 min, followed by three washes with ethanol. Finally, the product was dispersed in deionized water for subsequent use.

The Electron Microscopy

The scanning electron microscope (SEM) images was conducted at 10 kV and 10 mA using HITACHI S4800 microscope (Tokyo, Japan). The transmission electron microscope (TEM) images were conducted under 100 kV using HITACHI HT7700 microscope (Tokyo, Japan). The distribution and morphology of the elements were characterized by High-angle annular dark-field scanning TEM (HAADF-STEM) and an FEI Talos F200X electron microscope with energy-dispersive X-ray (EDX) spectroscopy.

The Animal Model

Mouse neuroblastoma cell line Neuro-2a was purchased from American Type Culture Collection (ATCC, Manassas, VA). Cells were cultured in MEM containing 10% FBS under recommended conditions (37 °C and 5% CO_2). All animal experimental procedures were undertaken in accordance with the guidelines for Laboratory Animal Welfare in Nanjing Medical University (http://iacuc.njmu.edu.cn:8080/article/list-10018.html). Ethical approval for all experiments was obtained from the Animal Ethics Committee at Nanjing First Hospital (DWSY-2101557). Female 4-5-week-old A/J mice (15–20 g) were purchased from Gempharmatech Co., Ltd. (Nanjing, China). The Neuro-2a xenograft-bearing mice model was established by the subcutaneous injection of 5×10^6 Neuro-2a cells (100 μL) into the lower right back of each mouse.

Uptake of MPNs in Neuro-2a Cells

To investigate the uptake of MPNs in Neuro-2a cells, the cells were seeded in 6-well plates with a density of 1.2×10^6 cells per well and incubated at 37 °C for 24 h before experiment. The cells were then treated with 100 μg·mL^{-1} MPNs and co-incubated for another 1, 2, 4, or 6 hours without light irradiation. After incubation, the cells were collected, fixed with 2.5% glutaraldehyde and made for TEM investigation. TEM micrographs were taken by a TEM (JEM-1230, JOEL, Tokyo, Japan) operating at 100 kV.

Cytotoxicity Assay

The cytotoxicity of MPNs was assessed using Neuro-2a cells. Briefly, the cells were seeded in 96-well plates with a density of 1×10^4 cells per well and incubated with different concentrations of MPNs (0–100 μg·mL^{-1}) for 24 h at 37°C. Subsequently, CCK-8 reagent (10 μL) was added to each well and incubated for 4 h. Finally, the absorbance was measured at 450 nm. Six parallel samples were carried out for each group.

Photothermal Therapy of MPNs in vitro

Neuro-2a cells were seeded into 96-well plates at 1×10^4 cells per well and incubated for 24 h. Then, different concentrations of MPNs were added to each well. After 6 h of incubation, each well was irradiated with laser for 5 min (808 nm, 1 W·cm^{-2}). After an additional 18 hours of incubation, 10 μL CCK-8 reagent was added to each well and incubated for 4 h. Finally, the absorbance was measured on a microplate reader at 450 nm. Cell viability was calculated. Six parallel samples were conducted for each group.

Anti-Tumor Efficacy of Combinatorial Losartan-PTT in vitro

To investigate the combinational therapeutic efficacy of MPNs-based PTT and losartan in vitro, Neuro-2a cells were seeded into 96-well plates at 1×10^4 cells per well and incubated for 24 h. Then, the cells were subjected to various treatments: (1) PBS, (2) PBS + NIR, (3) losartan, (4) MPNs, (5) MPNs + NIR, (6) MPNs + Los, and (7) MPNs + Los + NIR. The NIR treatment groups were irradiated with an 808 nm laser at a power density of 1 W·cm^{-2} for 5 min. After 18 h of incubation, cell viability was validated with CCK-8 kits.

LIVE/DEAD Viability Assay

For visual observation of cell survival, calcein AM/PI staining was used to distinguish living and dead cells. Following the various treatments employed in the previous experiment, the cell medium was discarded, the cells were washed with PBS. Subsequently, 100 μL calcein AM/PI solutions were added to each well. After 30 min of incubation at 37 °C in dark, the results were captured by a fluorescence microscope. Cells exhibiting green fluorescence were considered alive, whereas those with red fluorescence were classified as dead.

In vitro Immunogenic Cell Death Assays

To assess the impact of losartan on PTT-induced ICD, we quantified the surface expression of calreticulin and the release of ATP and HMGB1 based on consensus guidelines previously described by Kepp et al.[28] Neuro-2a cells were seeded on slides in a 12-well plate and incubated at 37 °C overnight. Then, the cells were treated with PBS, losartan, MPNs, or MPNs + losartan respectively for 6 h and subsequently triggered by 808 nm laser irradiation (1 W·cm^{-2}, 5 min). Following an additional 18 hours of incubation, the cells were fixed with 4% paraformaldehyde for 1 h and blocked with 1% BSA for 1 h at room temperature. Subsequently, the cells were incubated with the primary antibody of anti-calreticulin at 4 °C overnight. These cells were then treated by Alexa Fluor 594-labelled secondary antibody at room temperature for 1 h. After staining with DAPI, the cells were observed under a fluorescence microscope. The fluorescence intensity of cells labeled with calreticulin antibody and Alexa Fluor 594-labelled secondary antibody was quantified by flow cytometry.

The released HMGB1 and ATP were quantified using HMGB1 ELISA kit and ATP content assay kit, respectively. The Neuro-2a cells were seeded in a 12-well plate and incubated overnight. Then, the cells were treated with PBS, losartan, MPNs, or MPNs + losartan for 6 h and subsequently exposed to 808 nm laser irradiation (1 W·cm^{-2}, 5 min).

After continuing to incubate for 18 hours, the supernatant was collected and used to quantify the release of HMGB1 and ATP following the manufacturers' instructions.

Anti-Tumor Efficacy in vivo

Neuro-2a xenograft-bearing mice were randomly divided into 8 groups (n = 5) when the tumor volume reached to ≈100 mm^3: (1) PBS group; (2) PBS + NIR group; (3) MPNs group; (4) MPNs + NIR group; (5) MPNs + Los group; (6) MPNs + Los + NIR group; (7) Los group; (8) Los + NIR group. Mice in group 5, 6 and 8 were pretreated intravenously with losartan (20 μg per mouse) daily for one week. MPNs (100 μg per mouse) were intravenously injected into the mice of group 3–6 at day 0. At 24 h post injection, tumor sites of the NIR treatment groups were irradiated with an 808 nm laser at a power density of 2.0 $W \cdot cm^{-2}$ for 5 min. From 0–12 days, body weight and tumor width (X) and length (Y) were measured every two days. Tumor volumes (V) were calculated as follows: $V = (X^2Y)/2$. Relative tumor volume was calculated as V/V_0 (V_0 is the initial tumor volume).

Retention and Clearance of MPNs

The mesoporous Pt nanoparticles were labeled with Cy5.5, and two groups of mice were used for comparison: with or without losartan-pretreated. Both groups received intravenous injections of the Cy5.5-labeled MPNs via the tail vein. At 96 hours post-injection, we dissected the mice and collected their organs and tumors for optical imaging.

In vivo Biocompatibility of MPNs and Losartan

Blood samples and important organs (heart, liver, spleen, lung and kidney) were collected from the mice of the 8 groups at the end of the experiment. Serum creatinine (CRE), urea nitrogen (URE), uric acid, alanine aminotransferase (ALT), aspartate aminotransferase (AST) and alkaline phosphatase (ALP) were measured to assess kidney and liver function. The heart, liver, spleen, lung, and kidney were stained with hematoxylin and eosin (H&E) according to the manufacturer's instructions to investigate the organ morphology.

Peripheral Blood and Immunohistochemistry Analysis

At the conclusion of the experiment, peripheral blood was collected and stained with mouse mAbs for 30 min: CD45-PC7, CD3e-PE, CD4 Alexa Fluor 488, CD8a-A750, and PD-1-BV510. After staining, red cells were lysed and data were acquired using a Beckman Coulter Navios instrument. All the data was analyzed utilizing Kaluza Analysis Software. In addition, tumor tissues were harvested and fixed in formalin. IHC staining was carried out following the manufacturer's protocol. Paraffin-embedded sections underwent deparaffinization, and after antigen retrieval, slides were stained using Hematoxylin and Eosin (H&E) or monoclonal antibodies (mAbs) targeting CD31, α-SMA, PD-1, and calreticulin.

Statistical Analysis

All the measurements were performed at least three times, and the data were presented as mean ± SD. Ordinary one-way ANOVA was performed with SPSS 16.0 software. The criterion for statistical significance was denoted as $*p<0.05$, $**p<0.01$, and $***p<0.001$.

Results

SEM and TEM were employed to characterize the structures of the MPNs. The MPNs are well-dispersed and highly uniform in shape and size (Figure 1A). The high-magnification SEM image showed that the MPNs possess rough surface and uniform pores (Figure 1B). The high-magnification TEM image further confirmed the regularly spherical shape (Figure 1C) and uniform size of approximately of 75 nm (Figure 1D). EDX elemental mapping images showed that Pt elements uniformly distributed throughout the MPNs (Figure 1E). Furthermore, the clear lattice fringes observed in the high-resolution TEM (HRTEM) image (Figure 1F, G), which showed a lattice plane spacing of 0.1364 nm corresponding to Pt crystal, and the selected-area electron diffraction (SAED) pattern from Figure 1H demonstrated the high degree of crystallization of the pore walls.

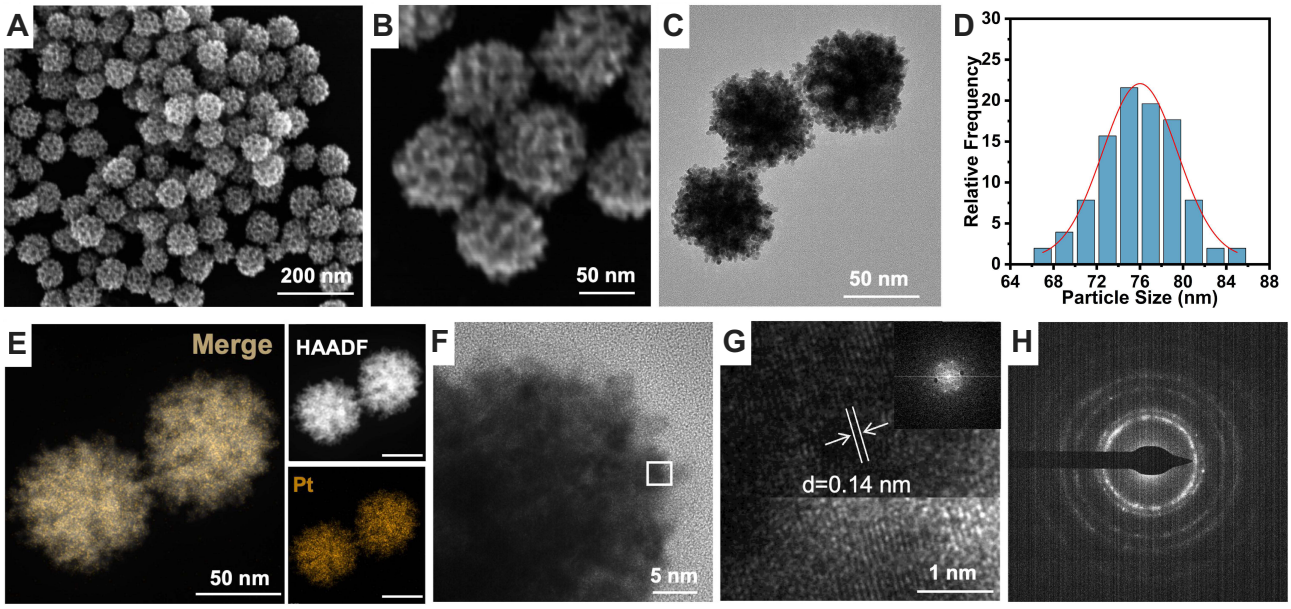

Figure 1 (**A** and **B**) SEM images, (**C**) TEM image, and (**D**) the histogram displaying the relative frequency of MPNs particle size. (**E**) EDX element mappings of MPNs. (**F** and **G**) HRTEM images of the MPNs and corresponding fast Fourier transform (FFT) image. (**H**) The corresponding selected area ED pattern of MPNs.

The effective cellular uptake of MPNs is critical for successful therapy. We observed the MPNs in Neuro-2a cells co-incubated with MPN for different time by TEM and found that the uptake of MPNs increased with prolonged co-incubation time, reaching its peak after 6 hours of co-incubation (Figure 2A-D). Furthermore, these TEM images

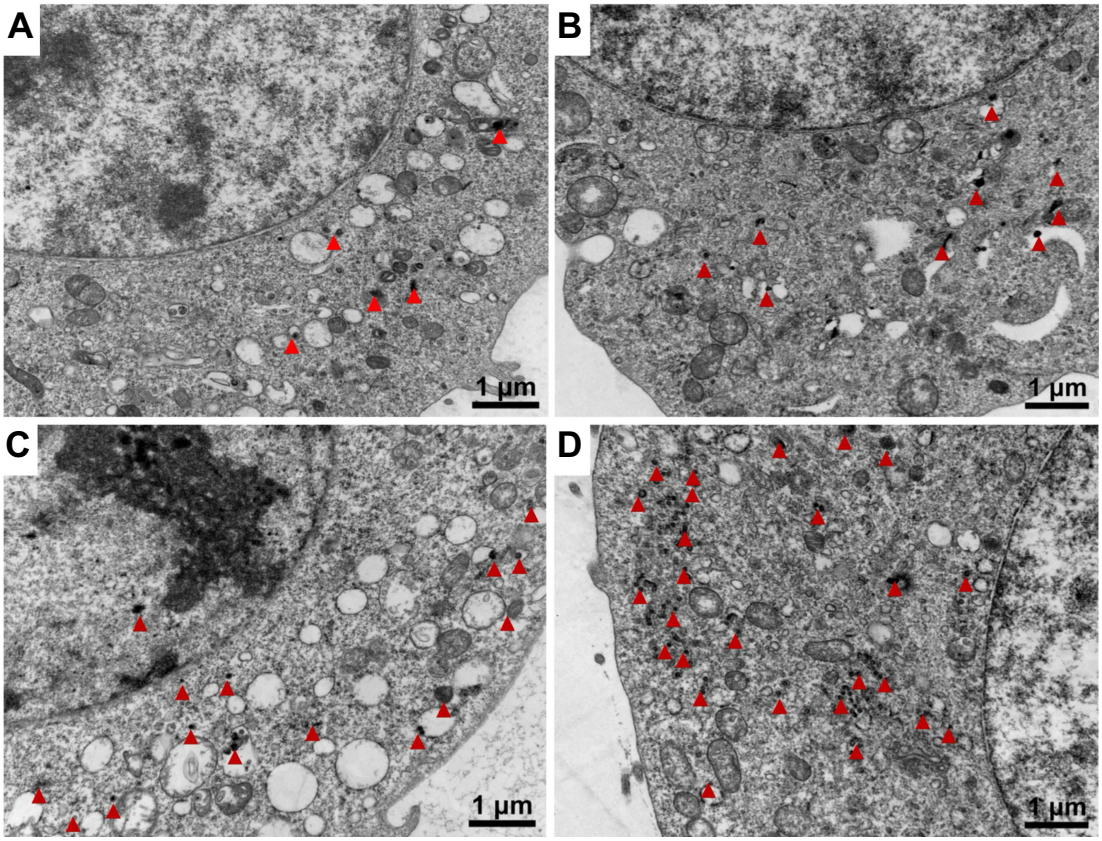

Figure 2 TEM image of MPNs uptake in Neuro-2a cells at different times points: (**A**) 1 h, (**B**) 2 h, (**C**) 4 h, and (**D**) 6 h. Red arrow indicates MPNs.

revealed that MPNs are uniformly distributed in the cytoplasm of Neuro-2a cells rather than being located outside the cells. This observation substantiates that MPNs were indeed absorbed by the cells.

The evaluation of biological safety was crucial for further treatment with MPNs. First, we investigated the in vitro cytotoxicity of the MPNs to evaluate the biological safety and biocompatibility. As the concentrations increased, MPNs exhibited minimal toxicity. As shown in Figure 3A, there was no obvious decrease in viability even after incubation with 100 μg·mL^{-1} MPNs for 24 h. After 48 h of incubation, the relative cell viability was above 73%, indicating that MPNs had excellent biocompatibility.

To assess the photothermal toxicity of MPNs in vitro, CCK-8 assay was performed on Neuro-2a cells preincubated with different concentrations of MPNs for 4 h and irradiated with an 808 nm at the power density of 1 W·cm^{-2} laser for 5 min. The PTT efficiency exhibited a concentration-dependent effect, with cell viability decreasing as the concentration of MPNs increased (Figure 3B). No significant changes in cell viability were observed after Neuro-2a cells were exposed to NIR irradiation without MPNs or co-incubated with 10 μg·mL^{-1} MPNs with NIR irradiation. However, the cell viability sharply decreased as concentrations increased from 25 μg·mL^{-1} to 100 μg·mL^{-1} with NIR irradiation. Specifically, when the concentration of MPNs was 100 μg·mL^{-1}, the viability was approximately 20% under 808 nm 1 W·cm^{-2} laser irradiation. In summary, the above results indicated that MPNs exhibit excellent performance as a photothermal therapy drug.

To assess the combinational therapeutic effects of MNPs and losartan, CCK-8 assay was performed on Neuro-2a cells after treatment with (1) PBS, (2) PBS +NIR, (3) losartan, (4) MPNs, (5) MPNs + NIR, (6) MPNs + Los, and (7) MPNs + Los + NIR, respectively. As shown in Figure 3C, the cell viability decreased significantly in MPNs + NIR group and

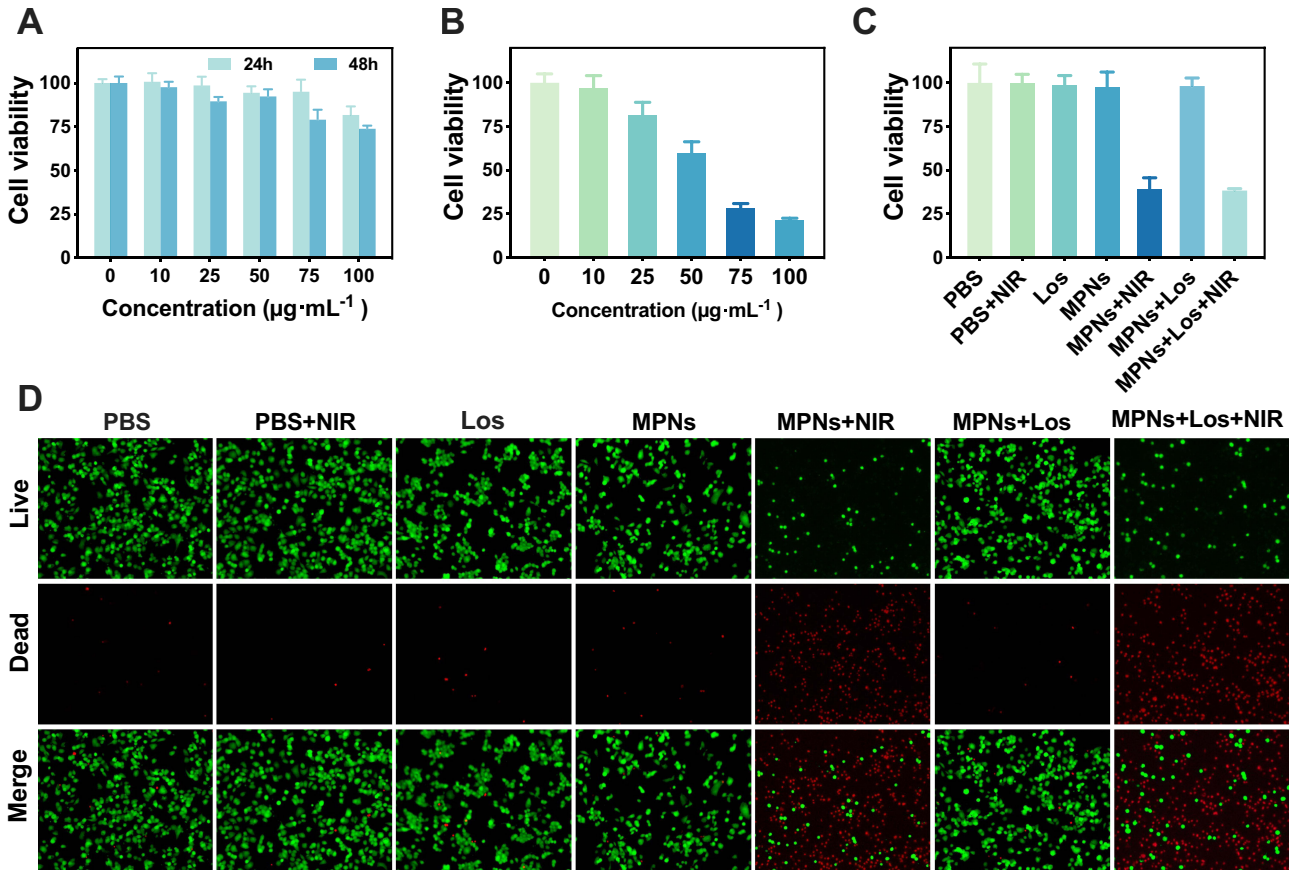

Figure 3 In vitro biocompatibility and therapeutic evaluation of MPNs. (**A**) Viability assay (CCK-8) of Neuro-2a cells after 24 h and 48 h of exposure to different concentrations of MPNs (0–100 μg·mL^{-1}). (**B**) The relative viabilities of Neuro-2a cells after treatment with MPNs at different concentrations (0–100 μg·mL^{-1}) and laser irradiation for 5 min (808 nm, 1 W·cm^{-2}). (**C**) The relative viabilities of Neuro-2a cells after different treatments with or without laser irradiation (808 nm, 1 W·cm^{-2}, 5 min). (**D**) Fluorescence microscopy images of live (green)/dead (red) cells after Neuro-2a cells received various treatments.

MPNs + Los+ NIR group, while no obvious decrease was observed in other groups. This was visually confirmed further by LIVE/DEAD cell staining, as shown in Figure 3D. It was found that the number of live cells (green) and dead cells (red) was similar in the PBS, PBS + NIR, Los, MPNs, and MPNs + Los groups. Moreover, dead cells increased significantly in MPNs + NIR group and MPNs + Los+ NIR group without obvious difference. We guess that this result is attributed to the primary function of losartan, which is to degrade the tumor matrix, with no direct killing effect on the tumor. Additionally, in the non-3D spheroid in vitro experiment, enhancing the penetration of nanoparticles into solid tumor has little promotion on PTT.

TME plays a vital role in influencing the outcome of immunologic therapy.[29] Due to the low mutation burden, the tumor immunogenicity of neuroblastoma is low. Neuroblastoma is a typical "cold" tumor, as the TME is usually immune suppressive in neuroblastoma.[13] How to change "cold" tumors to "hot" tumors is very important in neuroblastoma therapy. PTT has been reported to induce ICD and improve the suppressive TME. ICD promotes DC maturation, induces cytokines secretion and activates anti-tumor immunity.[11,30] It is characterized by calreticulin translocation, HMGB1 secretion and ATP release.[30,31] Thus, we evaluated the effects of MPNs, losartan, and laser on ICD by examining calreticulin exposure, HMGB1 and ATP release. Fluorescence images in Figure 4A showed no obvious calreticulin (red fluorescence) was observed in the PBS, PBS +NIR, Los, MPNs, and MPNs + Los groups. However, strong red fluorescence was observed in the MPNs + NIR group and MPNs + Los+ NIR group. The quantitative results of calreticulin assessed by flow cytometry were also consistent with the findings of fluorescence. As shown in Figure 4B, MPNs + NIR group and MPNs + Los+ NIR group exhibited more surface calreticulin than other five groups.

The release of HMGB1 is a crucial biomarker of ICD, as HMGB1 could induce the maturation of dendritic cells.[32] In this study, we discovered that after irradiation, MPNs and MPNs + losartan accelerated the release of HMGB1 dominantly compared to the PBS, PBS + NIR, Los, MPNs and MPNs + NIR group although the differences between

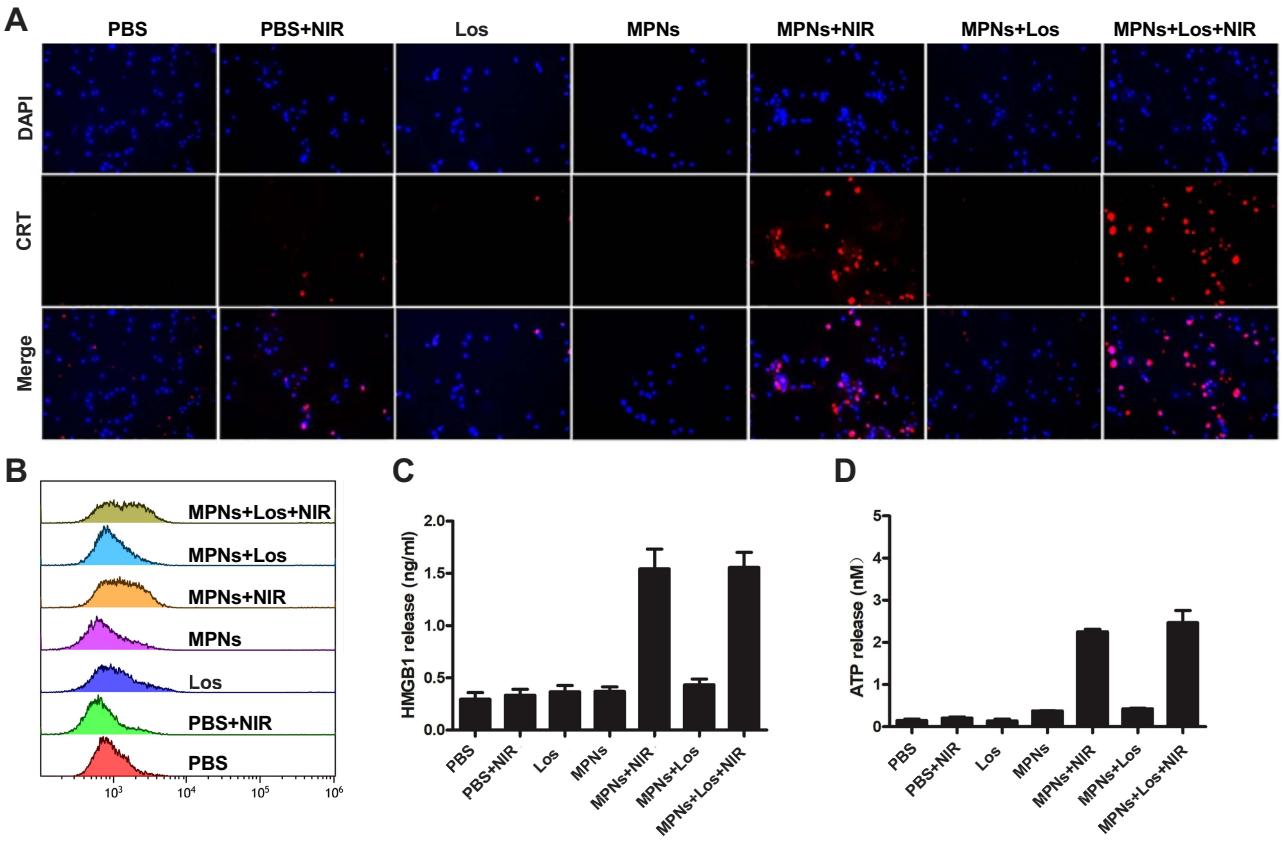

Figure 4 Evaluation of the effects of MPNs, losartan, and NIR on ICD. Cell surface exposure of calreticulin (CRT) upon treatment with PBS, PBS + NIR, losartan, MPNs, MPNs + NIR, MPNs + losartan, and MPNs + losartan + NIR groups determined by (**A**) fluorescence microscopy and (**B**) flow cytometry. (**C**) HMGB1 and (**D**) ATP released into the cellular medium after treatment (n = 3).

MPNs + NIR group and MPNs + Los+ NIR group were not statistically significant (Figure 4C). ATP released from dying tumor cells functions as a find-me signal and induces dendritic cells (DCs) to produce cytokines.[33] In the non-NIR and MPNs groups, ATP was released minimally. However, the MPNs + NIR group incubated with losartan resulted in the highest ATP release, surpassing that of the MPNs + NIR group (Figure 4D). The elevation in the surface expression of calreticulin, along with the accelerated release of HMGB1 and ATP, collectively confirms that MPNs-stimulated PTT could indeed induce ICD. In vitro, the experiment of ICD demonstrates that the Neuro-2a cells pretreated with MPNs + Los +NIR exhibited more surface calreticulin and released more HMGB1 and ATP. Furthermore, losartan has the additional effect of enhancing the release of ATP.

Encouraged by the good biocompatibility and therapeutic efficacy in vitro, we investigated the PTT efficacy by intravenous injection of MPNs and losartan into Neuro-2a tumor-bearing mice. As presented in Figure 5A, no significant variations were observed in the body weights of mice in all groups, indicating the low systemic toxicity of MPNs, losartan, and the photothermal treatment in vivo. As illustrated in Figure 5B, the PBS group, PBS + NIR group, Los group, Los + NIR group, MPNs group, and MPNs +Los group displayed a rapid tumor growth; while the group treated with MPNs + losartan presented a mild tumor growth. Most importantly, after receiving laser irradiation, tumor volume of MPNs group and MPNs + Los group decreased from day 0 to 6 and from day 7, and the tumor volume began to increase. In vivo, the MPNs + Los + NIR group exhibited the best anti-tumor efficacy, with a tumor suppression ratio of approximately 80%. This may be due to the normalization of the tumor vascular system and the effective improvement of tumor perfusion, which promoted the deposition of nanoparticles in the tumor. Voutouri et al demonstrated that depletion of hyaluronic acid and collagen decompresses blood vessels and improves perfusion.[34] And this means losartan could

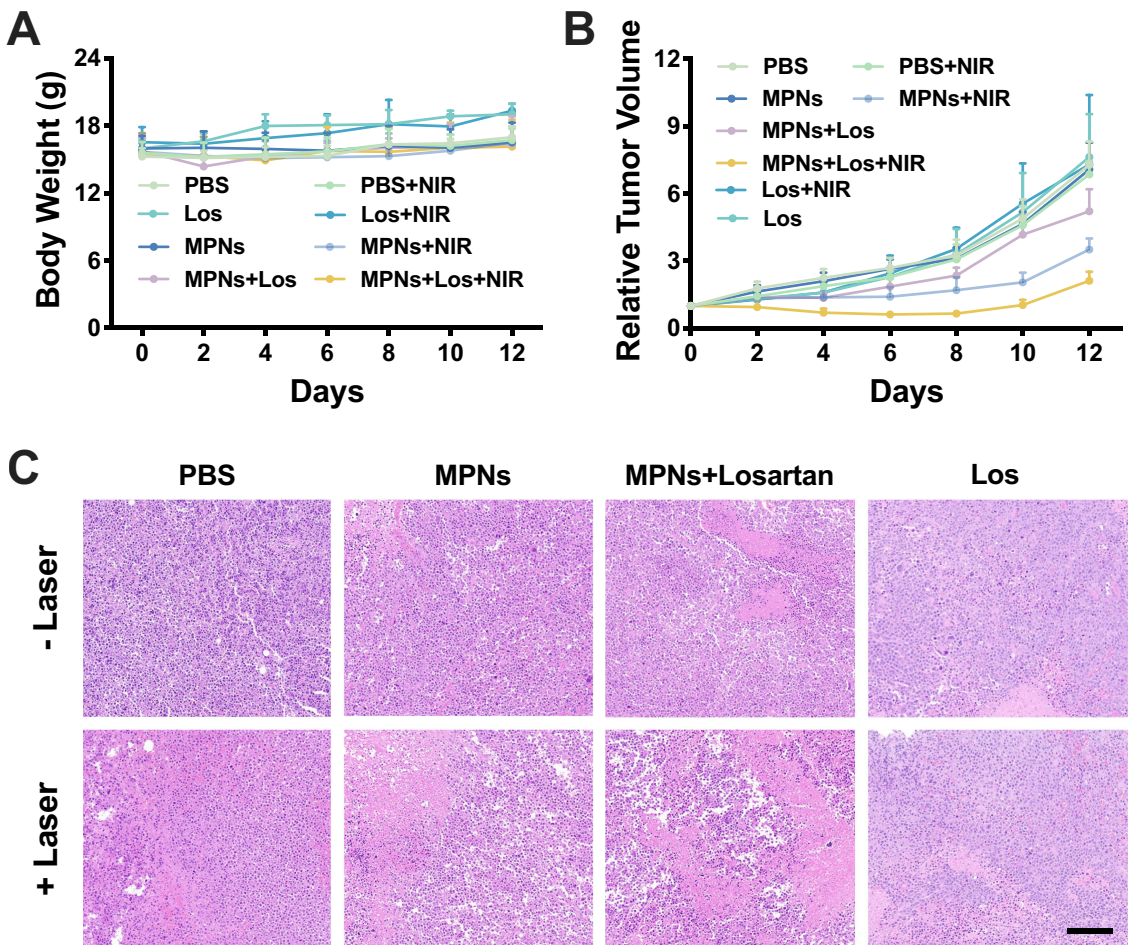

Figure 5 Antitumor effect of combining MPNs-based PTT and losartan in Neuro-2a xenograft-bearing mice. (**A**) Curves of mouse tumor volume with various treatments. (**B**) The body weights of Neuro-2a-bearing mice with different treatments. (**C**) Representative H&E sections of tumors after different treatments. Scale bar: 200 μm.

effectively inhibit fibroblast proliferation and collagen formation, which could significantly increase Neuro-2a tumor permeability and mesoporous platinum deposition within the tumor. As shown in Figure S1, strong fluorescence is evident in the tumors of both the MPNs group and the MPNs + Los group (96 hours after injection). Notably, the fluorescence intensity in the tumor tissues of MPNs pretreated with losartan exceeds that of the control group. This finding suggests that the removal of the intercellular matrix by losartan does not promote the expulsion of nanoparticles from the tumors.

H&E staining of tumor tissues was performed to investigate the efficacy of different therapeutic strategies. After different treatments, shrinkage of nuclei and nuclear fragmentation were observed to different extents. It is noticed that MPNs + NIR group and MPNs + Los+ NIR group displayed significant large areas of apoptotic or necrotic regions in tumor tissues (Figure 5C). In the group of MPNs + Los+ NIR, there were the most necrotic cells, suggesting MPNs + Los + NIR exhibited the best anti-tumor efficiency. The significant improvement of PTT effect in MPNs + Los+ NIR group is since losartan can degrade ECM and increase the penetration depth of MPNs in tumor.

Previous experiments suggested that losartan played a significant role in improving the TME and enhancing efficiency of PTT, and more ATP release also indicated its importance in ICD. Next, we studied the changes of immune factors in the blood of mice in different treatment groups to explore the role of losartan in tumor immune microenvironment. We evaluated the anti-tumor immunity using peripheral blood of mice after different treatments. $CD3^+$ T cell is a type of T lymphocyte characterized by the presence of the CD3 protein on its cell surface, and can be categorized into $CD4^+$ T cells and $CD8^+$ T cells.[35] They have the function of helping other immune cells coordinate immune responses and directly targeting and destroying abnormal cells. As shown in Figure 6A-C, $CD3^+$ and $CD4^+$ T cells were increased significantly after treatment with MPNs + NIR and MPNs + Los+ NIR. The $CD8^+$ T cells in the MPNs + Los + NIR group were also elevated compared to the control groups; however, a statistically significant difference was observed only when compared to the PBS + NIR group.

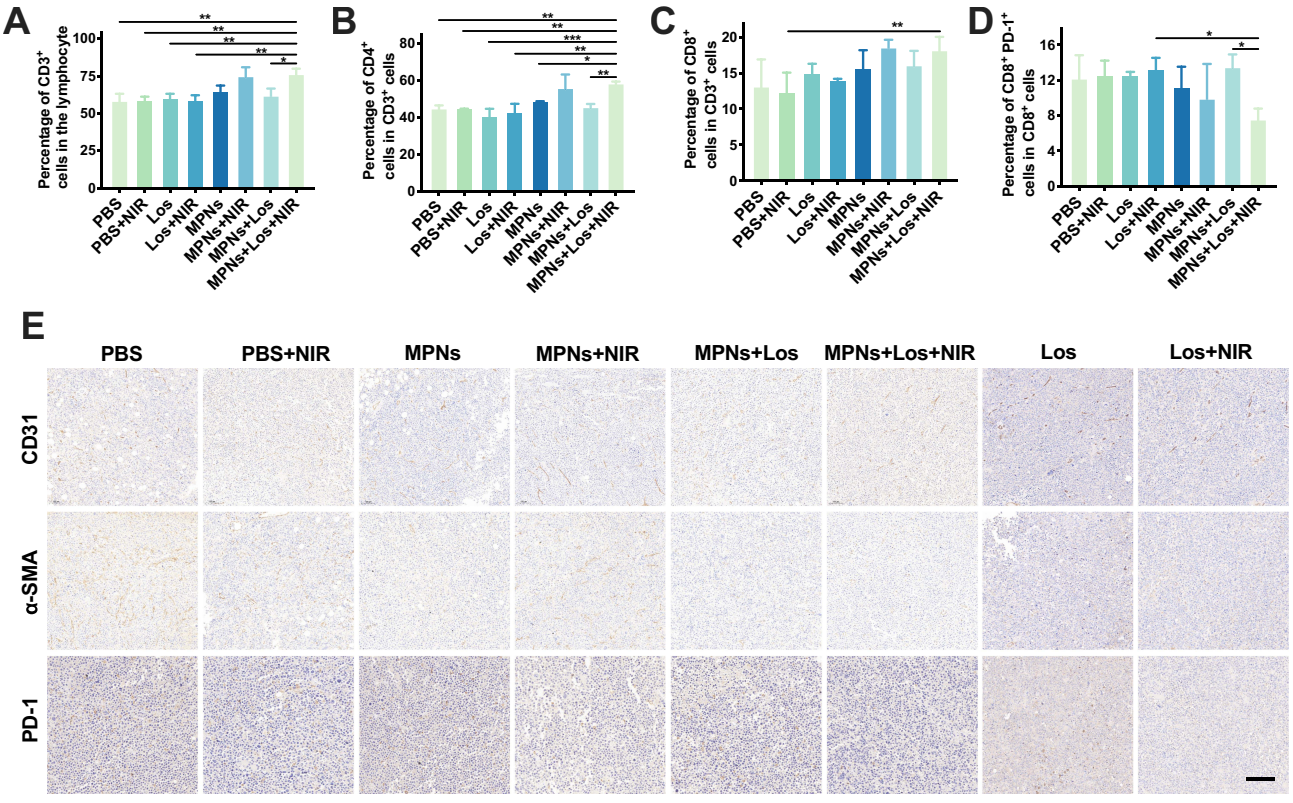

Figure 6 Immunostimulatory and tumor vascular inhibiting effects of combining PTT with losartan on Neuro-2a-bearing mice. (**A**) Percentage of $CD3^+$ cells in the lymphocyte, (**B**) Percentage of $CD4^+$ cells in $CD3^+$ cells, (**C**) Percentage of $CD8^+$ cells in $CD3^+$ cells, (**D**) Percentage of $CD8^+$ $PD\text{-}1^+$ cells in $CD8^+$ cells from peripheral blood of the mice after different treatments. (**E**) Representative IHC images in sections of tumors for CD31, α-SMA and PD-1 from mice with different treatments. Scale bar: 200 μm. The criterion for statistical significance was denoted as *p<0.05, **p<0.01.

In addition to tumor cells, all solid tumors contain many dense stromal cells, such as fibroblasts. Fibroblasts can activate/proliferate through transforming growth factor β1 (TGF-β1) signaling, resulting in a pro-fibroproliferative response rich in collagen fibers, hyaluronic acid, and other ECM molecules. Fibroblasts and others are deposited in the tumor extracellular matrix, which constitutes the structural support of the tumor, making it stiffer and thicker.[36] Additionally, the nearby blood vessels are compressed, further aggravating the poorly perfused and hypoxic environment of the tissue.[37] All these factors greatly limit the delivery and penetration of nanoparticles. Losartan, a type I angiotensin II receptor (AT1R) blocker (ARB) used to treat hypertension, inhibits TGF-β1 and thus the downstream pro-fibrotic pathway in fibroblasts. As α-SMA is a biomarker of activated CAFs,[38] we evaluated α-SMA and CD31 (a cytoplasmic pan-endothelial marker) expression in tumor after different treatments.[39] Analyzing post-treatment tumor pathology sections, we found that α-SMA expression was down-regulated after synergistic treatment with losartan (Figure 6E), which is essential for type 1 collagen synthesis, which was consistent with previous studies.[40] The expression of CD31 did not significantly decrease after different treatments (Figure 6E), which may be related to the slow process of vascular remodeling. Although losartan decreased the pressure of tumor stroma, it may not yet have a significant effect on vascular structure in a short period of time.

In addition, immune checkpoint blockade (ICB) has become a hot topic in cancer precision therapy. It reinvigorates the antitumor response by blocking co-inhibitory signaling pathways, thus contributing to the elimination of cancer cells by releasing cytokines and cytotoxic granules from effector T cells. In cancer, overexpression of PD-1 assists cancer cells in evading damage by the immune system. The IHC results of our study revealed that there were fewer PD-1^+ cells in tumors in the MPNs + NIR and MPNs + Los +NIR group than in the other groups (Figure 6E). $CD8^+$PD-1^+ cells are $CD8^+$ T cells that express programmed cell death protein 1(PD-1) on their surfaces.[41] The $CD8^+$PD-1^+ cells in the MPNs + Los + NIR group were significantly fewer than those in the Los + NIR group and the MPNs + Los group. However, there was no statistically significant difference in the reduction when compared to the MPNs + NIR group (Figure 6D). A reduction in PD-1^+ cells indicated the enhanced tumor eliminating ability of cytotoxic T cells.

To assess the biosafety of different treatments, we conducted an examination of toxicity. The major organs of mice, including the heart, liver, spleen, lung, and kidney, were removed from each group and stained with H&E at the end of the experiment. According to the H&E staining results, none of the treatment groups showed apparent organ damage, including inflammation and necrosis (Figure 7A). Additionally, the blood biochemical indexes were analyzed at the end of the experiment. As shown in Figure 7B-G, ALP, BUN, Cr and uric acid did not change significantly after different treatments compared to the PBS group. However, we observed that AST levels were significantly higher in the MPNs + NIR group compared to the PBS group. Conversely, AST levels were significantly lower in the group injected with losartan when compared to the MPNs + NIR group. Additionally, the ALT levels in the MPNs + Los + NIR group were significantly lower than those in both the MPNs + Los group and the MPNs + NIR group. As AST and ALT serve as markers for liver function, while BUN, creatinine, and uric acid are indicators of kidney function, the serum biochemical results indicated that the various treatments did not lead to significant toxicity in either the liver or the kidneys. Furthermore, losartan could contribute to the recovery of liver function decline induced by MPNs and laser treatment. The results presented above demonstrate that MPNs exhibit favorable biocompatibility and significant potential for in vivo applications.

Conclusion

We found that losartan significantly enhanced the photothermal therapeutic efficacy of MPNs in a neuroblastoma mouse model by reducing CAFs in solid tumors. In addition to inducing tumor necrosis and apoptosis through elevated temperature, this study confirmed the immune activation effect of PTT: tumor cells exhibited clear signs of ICD, T lymphocytes in the peripheral blood of PTT-treated mice increased significantly, and immune checkpoint molecule PD-1 levels decreased, particularly in the MPNs + Los + NIR group. Our in vivo experiment demonstrated that the group treated with MPNs, losartan, and NIR light had the best effect. Furthermore, losartan showed a protective effect on liver function in mice undergoing MPNs-based PTT. However, our evaluation of the tumor immune status following photothermal immunotherapy was not comprehensive, and investigating its efficacy in tumor recurrence models will be a focus of future research.

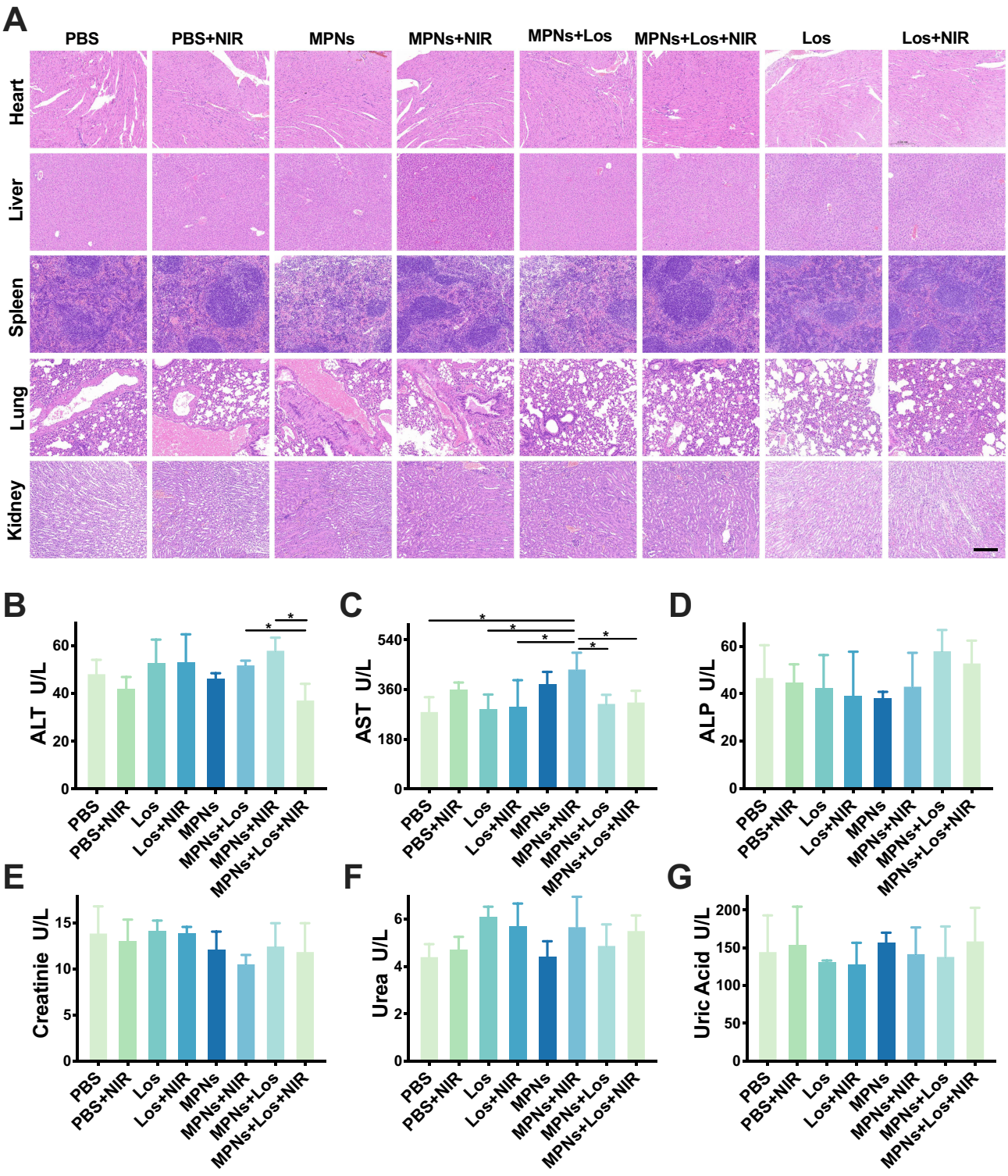

Figure 7 Biosafety analysis of combinational treatment of MPNs-based PTT and Losartan. (**A**) Representative H&E staining in sections of heart, liver, spleen, lung and kidney from different groups to assess the biosafety. (Scale bar, 200 μm). Serum ALT (**B**), AST (**C**), ALP (**D**), creatinine (**E**), Urea (**F**) and Uric Acid (**G**) from different groups were used to evaluate the effects of different treatments on liver and kidney function. The criterion for statistical significance was denoted as *p<0.05.

Acknowledgments

This work was supported by Jiangsu Provincial Medical Key Discipline Cultivation Unit (JSDW202247), Jiangsu Provincial Key Research and Development Special Fund (BE2017612), National Natural Science Foundation of China (82003532, 81901806), and Nuclear Medicine Laboratory Open Project (2021HYX009). We would like to thank

Dr. Xuzhi Shi for his help in modifying fluorescence on mesoporous platinum nanoparticles during the supplementary experiment.

Disclosure

The authors report no conflicts of interest in this work.

References

1. Maris JM. Recent advances in neuroblastoma. *N Engl J Med*. 2010;362(23):2202–2211. doi:10.1056/NEJMra0804577
2. Maris JM, Hogarty MD, Bagatell R, Cohn SL. Neuroblastoma. *Lancet*. 2007;369(9579):2106–2120. doi:10.1016/S0140-6736(07)60983-0
3. Pearson AD, Pinkerton CR, Lewis IJ, et al. High-dose rapid and standard induction chemotherapy for patients aged over 1 year with stage 4 neuroblastoma: a randomised trial. *Lancet Oncol*. 2008;9(3):247–256. doi:10.1016/S1470-2045(08)70069-X
4. Matthay KK. Chemotherapy for neuroblastoma: does it hit the target? *Lancet Oncol*. 2008;9(3):195–196. doi:10.1016/S1470-2045(08)70046-9
5. Vollmer K, Gfroerer S, Theilen TM, et al. Radical surgery improves survival in patients with stage 4 neuroblastoma. *World J Surg*. 2018;42(6):1877–1884. doi:10.1007/s00268-017-4340-9
6. Holmes K, Potschger U, Pearson ADJ, et al. Influence of surgical excision on the survival of patients with stage 4 high-risk neuroblastoma: a report from the HR-NBL1/SIOPEN study. *J Clin Oncol*. 2020;38(25):2902–2915. doi:10.1200/JCO.19.03117
7. Furman WL, McCarville B, Shulkin BL, et al. Improved outcome in children with newly diagnosed high-risk neuroblastoma treated with chemoimmunotherapy: updated results of a Phase II study using hu14.18K322A. *J Clin Oncol*. 2022;40(4):335–344. doi:10.1200/JCO.21.01375
8. Heitzeneder S, Bosse KR, Zhu Z, et al. GPC2-CAR T cells tuned for low antigen density mediate potent activity against neuroblastoma without toxicity. *Cancer Cell*. 2022;40(1):53–69e59. doi:10.1016/j.ccell.2021.12.005
9. Li X, Lovell JF, Yoon J, Chen X. Clinical development and potential of photothermal and photodynamic therapies for cancer. *Nat Rev Clin Oncol*. 2020;17(11):657–674. doi:10.1038/s41571-020-0410-2
10. Sweeney EE, Cano-Mejia J, Fernandes R. Photothermal therapy generates a thermal window of immunogenic cell death in neuroblastoma. *Small*. 2018;14(20):e1800678. doi:10.1002/smll.201800678
11. Shukla A, Cano-Mejia J, Andricovich J, Burga RA, Sweeney EE, Fernandes R. An engineered Prussian blue nanoparticles-based nanoimmunotherapy elicits robust and persistent immunological memory in a TH-MYCN neuroblastoma model. *Adv Nanobiomed Res*. 2021;1(8). doi:10.1002/anbr.202100021
12. Ma J, Li N, Wang J, Liu Z, Han Y, Zeng Y. In vivo synergistic tumor therapies based on copper sulfide photothermal therapeutic nanoplatforms. *Exploration*. 2023;3(5):20220161. doi:10.1002/EXP.20220161
13. Pelizzo G, Veschi V, Mantelli M, et al. Microenvironment in neuroblastoma: isolation and characterization of tumor-derived mesenchymal stromal cells. *BMC Cancer*. 2018;18(1):1176. doi:10.1186/s12885-018-5082-2
14. Yang D, Liu J, Qian H, Zhuang Q. Cancer-associated fibroblasts: from basic science to anticancer therapy. *Exp Mol Med*. 2023;55(7):1322–1332. doi:10.1038/s12276-023-01013-0
15. Bhatt HN, Diwan R, Borrego EA, et al. A photothermal driven chemotherapy for the treatment of metastatic melanoma. *J Control Release*. 2023;361:314–333. doi:10.1016/j.jconrel.2023.08.005
16. Fang T, Zhang J, Zuo T, et al. Chemo-photothermal combination cancer therapy with ros scavenging, extracellular matrix depletion, and tumor immune activation by telmisartan and diselenide-paclitaxel prodrug loaded nanoparticles. *ACS Appl Mater Interfaces*. 2020;12(28):31292–31308. doi:10.1021/acsami.0c10416
17. Insua-Rodriguez J, Oskarsson T. The extracellular matrix in breast cancer. *Adv Drug Deliv Rev*. 2016;97:41–55. doi:10.1016/j.addr.2015.12.017
18. Stylianopoulos T, Jain RK. Combining two strategies to improve perfusion and drug delivery in solid tumors. *Proc Natl Acad Sci*. 2013;110(46):18632–18637. doi:10.1073/pnas.1318415110
19. Stylianopoulos T, Munn LL, Jain RK. Reengineering the physical microenvironment of tumors to improve drug delivery and efficacy: from mathematical modeling to bench to bedside. *Trends Cancer*. 2018;4(4):292–319. doi:10.1016/j.trecan.2018.02.005
20. Laronha H, Caldeira J. Structure and function of human matrix metalloproteinases. *Cells*. 2020;9(5):1076. doi:10.3390/cells9051076
21. Diop-Frimpong B, Chauhan VP, Krane S, Boucher Y, Jain RK. Losartan inhibits collagen I synthesis and improves the distribution and efficacy of nanotherapeutics in tumors. *Proc Natl Acad Sci*. 2011;108(7):2909–2914. doi:10.1073/pnas.1018892108
22. Chauhan VP, Martin JD, Liu H, et al. Angiotensin inhibition enhances drug delivery and potentiates chemotherapy by decompressing tumour blood vessels. *Nat Commun*. 2013;4(1):2516. doi:10.1038/ncomms3516
23. Nakai Y, Isayama H, Ijichi H, et al. Inhibition of renin-angiotensin system affects prognosis of advanced pancreatic cancer receiving gemcitabine. *Br J Cancer*. 2010;103(11):1644–1648. doi:10.1038/sj.bjc.6605955
24. Liu H, Naxerova K, Pinter M, et al. Use of angiotensin system inhibitors is associated with immune activation and longer survival in nonmetastatic pancreatic ductal adenocarcinoma. *Clin Cancer Res*. 2017;23(19):5959–5969. doi:10.1158/1078-0432.CCR-17-0256
25. Li L, Zhu G, Xu W, et al. Construction of mPt/ICG-alphaA nanoparticles with enhanced phototherapeutic activities for multidrug-resistant bacterial eradication and wound healing. *Nanoscale*. 2023;15(33):13617–13627. doi:10.1039/D3NR02010J
26. Zhang J, Xu Z, Li Y, et al. Theranostic mesoporous platinum nanoplatform delivers halofuginone to remodel extracellular matrix of breast cancer without systematic toxicity. *Bioeng Transl Med*. 2023;8(4):e10427. doi:10.1002/btm2.10427
27. Fu B, Dang M, Tao J, Li Y, Tang Y. Mesoporous platinum nanoparticle-based nanoplatforms for combined chemo-photothermal breast cancer therapy. *J Colloid Interface Sci*. 2020;570:197–204. doi:10.1016/j.jcis.2020.02.051
28. Kepp O, Senovilla L, Vitale I, et al. Consensus guidelines for the detection of immunogenic cell death. *Oncoimmunology*. 2014;3(9):e955691. doi:10.4161/21624011.2014.955691
29. Galon J, Costes A, Sanchez-Cabo F, et al. Type, density, and location of immune cells within human colorectal tumors predict clinical outcome. *Science*. 2006;313(5795):1960–1964. doi:10.1126/science.1129139

30. Balakrishnan PB, Ledezma DK, Cano-Mejia J, et al. CD137 agonist potentiates the abscopal efficacy of nanoparticle-based photothermal therapy for melanoma. *Nano Res*. 2022;15(3):2300–2314. doi:10.1007/s12274-021-3813-1
31. Ledezma DK, Balakrishnan PB, Shukla A, et al. Interstitial photothermal therapy generates durable treatment responses in neuroblastoma. *Adv Healthc Mater*. 2022;11(20):e2201084. doi:10.1002/adhm.202201084
32. Wiernicki B, Maschalidi S, Pinney J, et al. Cancer cells dying from ferroptosis impede dendritic cell-mediated anti-tumor immunity. *Nat Commun*. 2022;13(1):3676. doi:10.1038/s41467-022-31218-2
33. Silva-Vilches C, Ring S, Mahnke K. ATP and its metabolite adenosine as regulators of dendritic cell activity. *Front Immunol*. 2018;9:2581. doi:10.3389/fimmu.2018.02581
34. Voutouri C, Polydorou C, Papageorgis P, Gkretsi V, Stylianopoulos T. Hyaluronan-derived swelling of solid tumors, the contribution of collagen and cancer cells, and implications for cancer therapy. *Neoplasia*. 2016;18(12):732–741. doi:10.1016/j.neo.2016.10.001
35. Yakirevich E, Resnick MB. Regulatory T lymphocytes: pivotal components of the host antitumor response. *J Clin Oncol*. 2007;25(18):2506–2508. doi:10.1200/JCO.2007.11.3191
36. Evans A, Armstrong S, Whelehan P, et al. Can shear-wave elastography predict response to neoadjuvant chemotherapy in women with invasive breast cancer? *Br J Cancer*. 2013;109(11):2798–2802. doi:10.1038/bjc.2013.660
37. Martin JD, Fukumura D, Duda DG, Boucher Y, Jain RK. Reengineering the tumor microenvironment to alleviate hypoxia and overcome cancer heterogeneity. *Cold Spring Harb Perspect Med*. 2016;6(12):a027094.
38. Itoh G, Takagane K, Fukushi Y, et al. Cancer-associated fibroblasts educate normal fibroblasts to facilitate cancer cell spreading and T-cell suppression. *Mol Oncol*. 2022;16(1):166–187. doi:10.1002/1878-0261.13077
39. Reis RM, Reis-Filho JS, Longatto Filho A, Tomarev S, Silva P, Lopes JM. Differential Prox-1 and CD 31 expression in mucousae, cutaneous and soft tissue vascular lesions and tumors. *Pathol Res Pract*. 2005;201(12):771–776. doi:10.1016/j.prp.2005.08.010
40. Han C, Liu T, Yin R. Biomarkers for cancer-associated fibroblasts. *Biomark Res*. 2020;8(1):64. doi:10.1186/s40364-020-00245-w
41. Gros A, Parkhurst MR, Tran E, et al. Prospective identification of neoantigen-specific lymphocytes in the peripheral blood of melanoma patients. *Nat Med*. 2016;22(4):433–438. doi:10.1038/nm.4051